JOURNAL OF MATERIALS SCIENCE **39** (2004) 4533–4541

Mechanical and microstructural investigations of nitrided Fe-Cr layers

M. SENNOUR
GEMPPM, UMR CNRS 5510, Bât. B. Pascal, INSA de Lyon, F-69621 Villeurbanne Cedex, France

C. JACQ
GEMPPM, UMR CNRS 5510, Bât. B. Pascal, INSA de Lyon, F-69621 Villeurbanne Cedex, France; SNECMA, Site de Villaroche, 77550 Moissy Cramayel, France

C. ESNOUF*
GEMPPM, UMR CNRS 5510, Bât. B. Pascal, INSA de Lyon, F-69621 Villeurbanne Cedex, France
E-mail: claude.esnouf@insa-lyon.fr

Nano-indentation measurements were carried out on nitrided Fe-Cr alloys (1 and 3 wt% Cr) in order to determine local micro-mechanical properties. The method recently developed on nitrided 32CrMoV13 steel was applied to the Fe-Cr alloys. Evolution of micro-yield stress through the nitrided layer was correlated to microstructural parameters (volume fraction of CrN precipitates, diameter of precipitates, etc.) investigated and statistically analyzed by transmission electron microscopy (TEM). The results show that the mechanical behavior of the nitrided layer for both alloys studied can be described using the Orowan model of precipitation strengthening.

1. Introduction

Nitriding of iron and steel produces phases that enhance the tribological and mechanical properties of these materials [1]. This treatment also induces a mechanical profile through the nitrided layer whose the determination is a problem.

In order to determine micro-mechanical properties of nitrided layers and in particular micro-yield stress (MYS), which is more suitable than micro-hardness for estimating the endurance limit in the case of mechanical fatigue of high strength steels, it is necessary to perform local measurements such as nano-indentation [2].

For this reason, several studies [3–5] were carried out in order to develop computational methods to derive quantitative mechanical properties from nano-indentation data. Thus, Elghazal *et al.* [3] developed a procedure based on finite element (FE) simulation of the nano-indentation test from the determination of the strain-hardening law $\sigma(\varepsilon_p)$ where ε_p is the plastic deformation. Subsequently, the method was improved by Jacq *et al.* [4] in order to take account of residual stresses generated within the layer during surface treatment.

On the other hand, full comprehension of mechanical behavior of nitrided layers, in particular the existence of a mechanical properties profile, requires microstructural investigations at different depths. In the case of nitrided Fe-M (M = Cr, V, Ti, ...) binary alloys considered as a model for complex microstructure steels, the precipitation of fine semi-coherent M-N nitrides is responsible for mechanical properties improvement [6]. The main purpose of this work on nitrided Fe-Cr alloys is to correlate the evolution of the MYS estimated by nano-indentation to microstructural parameters of CrN precipitates investigated by TEM.

2. Experimental

2.1. Materials

Pure Fe-Cr alloy (1 and 3 wt% Cr) samples were supplied by Ecole des Mines de Saint-Etienne. Their chemical composition is given in Table I. Before nitriding, specimens ($30 \times 10 \times 1$ mm^3) were annealed at 923 K for 3 h in silica sealed capsules. Nitriding was performed in a gas mixture (NH_3, N_2, N_2O) at 823 K in a BMI furnace (details of the treatment sequences are given elsewhere [7]). The micro-hardness and the nitrogen concentration profiles thus obtained are shown in Fig. 1.

2.2. Nano-indentation tests

Nano-indentation measurements were performed using a Nano-Instruments Model II nano-indenter. The apparatus was equipped with a spherical-tipped indenter with a radius of approximately 105 μm. In accordance with the procedure set up by Elghazal *et al.* [3],

*Author to whom all correspondence should be addressed.

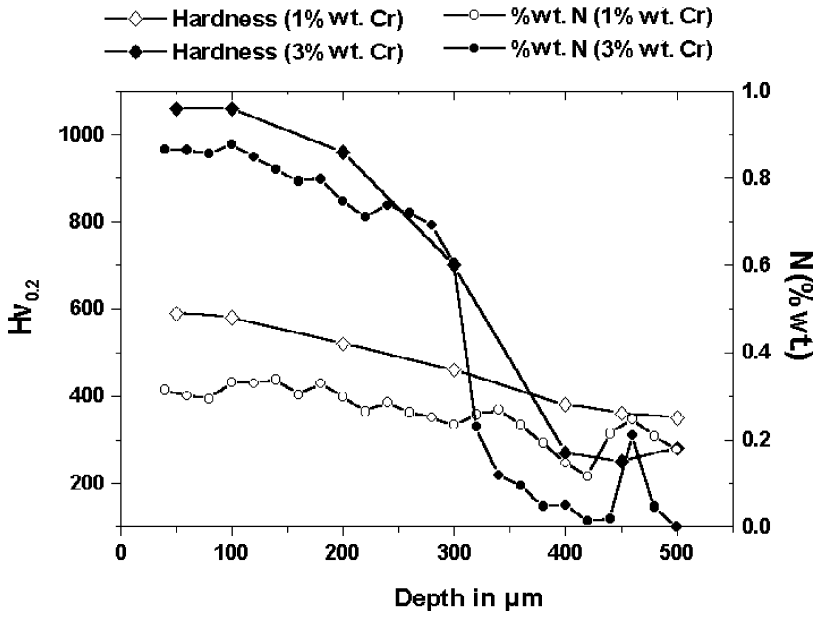

Figure 1 (a) Vickers micro-hardness ($Hv_{0.2\,kg}$) obtained after a 14 h nitriding at 823 K for both alloys studied through the 1 mm sample thickness and (b) Nitrogen concentration profiles for the half thickness (CAMEBAX SX microprobe).

the nano-indentation test consisted of successive loading/unloading cycles at increasing maximal load F_{max} (50, 150, 250, 450 and 650 mN), in order to characterize the overall plasticity within stressed region beneath the contact. Loading/unloading cycles were performed perpendicular to the nitrided surface, i.e., on cross-sectional specimens (1 mm thick) which were mechanically polished with a final stage of 1 μm diamond. After each indentation cycle, the difference in displacement before loading and after unloading, also called the residual displacement (δr) was measured. Cumulative displacement for each maximal applied force was calculated according to equations such as:

$$dr_{(250\,mN)} = \delta r_{(250\,mN)} + \delta r_{(150\,mN)} + \delta r_{(50\,mN)} \quad (1)$$

For each alloy, 10 series of 4 indentations localized at different depths below the surface (100, 200, 300 and 400 μm) were performed. The $dr = f(F_{max})$ response was drawn using an average value of 10 measurements.

As mentioned in the Introduction, the main interest for nitrided steels submitted to mechanical fatigue is the estimation of the limit of endurance in relation with MYS. This latter corresponds to the first irreversible dislocations movement and is classically deduced from the strain-hardening law $\sigma(\varepsilon_p)$. In rolling contact fatigue applications, it has been shown that a MYS with a proof strain of 0.002% results in a satisfactory estimation of the endurance limit of high strength steels [5].

Since the nano-indentation test does not give $\sigma(\varepsilon_p)$ response, the determination of MYS consisted in the simulation of the nano-indentation test with a given strain-hardening law, followed by the comparison to experimental results with continuous improving of the simulation parameters until reaching the best match between both approaches. A previous study [3] showed that the stress-plastic strain hardening behavior of a nitrided chromium steel (32CrMoV13) containing 3 wt% Cr was well suited to Swift's law:

$$\sigma = B(C + \varepsilon_p)^n \quad (2)$$

where only the B parameter is variable with depth, the two others C and n being fixed and close to 16 and 0.067, respectively. Furthermore, taking into account residual stresses, Jacq *et al.* [4] established a power law describing indirectly the variation of the residual displacement (dr) as a function of the load:

$$dr = \alpha[2\tau_0 - B(C + \varepsilon_p)^n]^\beta \quad (3)$$

where τ_0 represents the principal shear stress due to the elastic contact between the indenter and the sample and consequently it depends on the radius of the indenter as well as the load, whereas α and β depend only on the load. Therefore, for each load, the exploitation of the nano-indentation tests consists of the determination of the B value that fits the best the experimental results. MYS is then directly calculated using relation (2) for a 0.002% proof strain.

The similarity of microstructures and micro-hardness values of the 32CrMoV13 steel and the studied alloys [8] makes application of the same procedure suitable for determination of micro-mechanical properties of the latter.

TABLE I Chemical composition (% wt) of both studied Fe-Cr alloys

	Cr	C	S	O	N
Alloy 1	0.95	<0.0010	<0.0010	<0.0010	<0.0010
Alloy 2	2.98	<0.0010	<0.0010	<0.0010	<0.0010

2.3. Microstructural characterization

TEM sample preparation consisted of mechanical abrasion followed by chemical electropolishing (46.5%

butoxyethanol, 46.5% methanol, 7% perchloric acid) using a Struers-Tenupol 5 apparatus. According to the nano-indentation results, thin foils were sliced at different depths parallel to the nitrided surface (100, 300 and 400 μm).

TEM investigations were performed on a JEOL 2010F field emission gun microscope equipped with an Oxford Instruments energy dispersive X-ray (EDX) analyzer and an EELS Gatan Digi-PEELS 776 spectrometer. For each depth, statistical analysis were performed on several hundred of precipitates distributed throughout the thin foils. However, in the case of the Fe-3 wt% Cr alloys where the regions close to the surface are mostly transformed by discontinuous (lamellar) precipitation of CrN (Fig. 2a), quantitative studies were exclusively made on untransformed regions containing only continuous (submicroscopic) precipitation of CrN. For this alloy, indentation tests were performed solely on these untransformed areas.

Furthermore, CrN nitrides have a disc shape and are divided into three orthogonal families with the Baker-Nutting orientation relationship with respect to the iron matrix (Fig. 2b):

$$(100)_{CrN}//(100)_{Fe}; \quad [110]_{CrN}//[001]_{Fe} \qquad (4)$$

Hence, when observed along the $\langle 001 \rangle_{Fe}$ zone axis, the two families perpendicular to the foil plane are projected on their diameter and appear as rods whose lengths can be assimilated to the precipitates diameters. However, for a reliable quantitative study, we must take into account of the cutting of some precipitates during the thin foil preparation. For this reason, mean projected

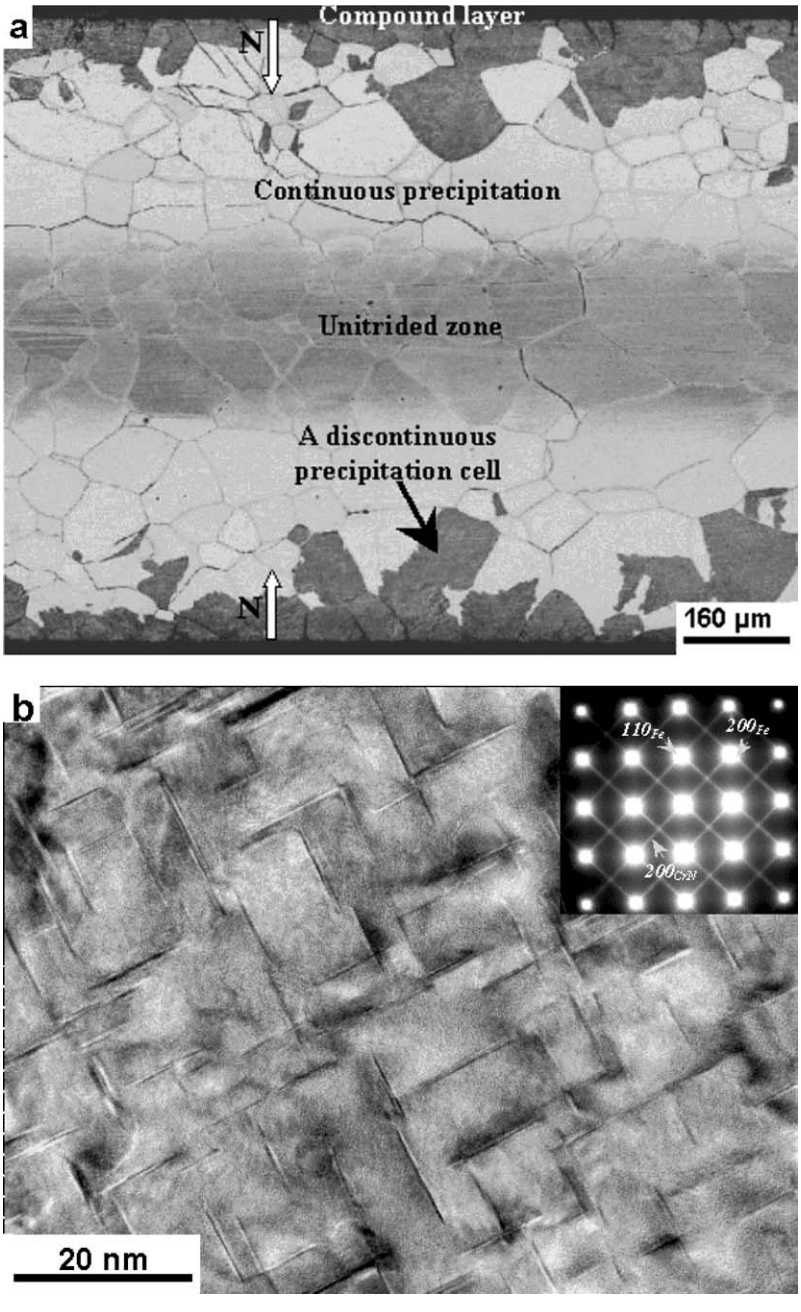

Figure 2 (a) Cross-section SEM view of the nitrided surface in the Fe-3 wt% alloys. Superficial regions are transformed by CrN discontinuous precipitation (dark zones). (b) $[001]_{Fe}$ zone axis TEM micrograph showing submicroscopic CrN precipitates. The indexation of the diffraction pattern is coherent with the Baker-Nutting relationship.

length on TEM micrographs does not exactly represent the true mean diameter of precipitates. Hence, in order to consider this effect, the measured precipitates mean diameter has been corrected using a geometric computational simulation on *Mathcad* software [9]. Comparison between measured and corrected values indicates that the omission of precipitates cutting effect leads to an underestimation of the precipitates mean diameter (Table II).

In view of all these considerations, main steps of the quantification process were the following:

1. For each analyzed area, the precipitates number (n) and their true mean diameter (D) are determined using image processing software.
2. The mean thickness of precipitates (t_p) is estimated from HRTEM Fourier-filtered images (Fig. 3a and b). HRTEM images were performed along the

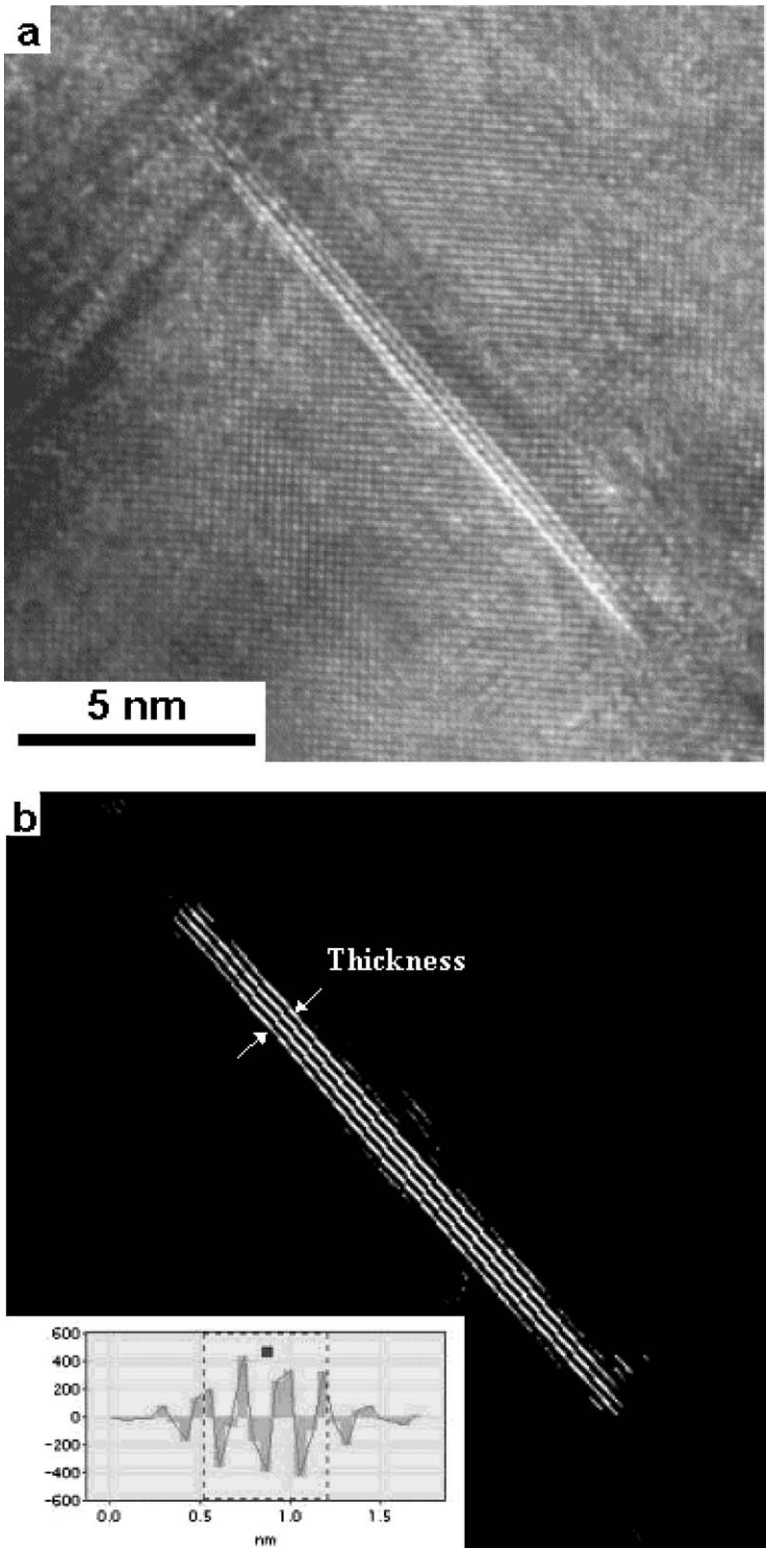

Figure 3 (a) HRTEM image along [002] zone axis of a submicroscopic CrN precipitates, (b) Image of (200) CrN planes. Image is formed by the selection (Gaussien mask) of the 200 and −200 spots on the Fourier transform of image (a). (insert corresponds to the transverse contrast profile of precipitate image).

TABLE II Measured and corrected means diameters of precipitates

Depth (μm)	$D_{meas.}$(nm)	$D_{corr.}$ (nm)
Fe-1 wt% Cr		
100	11.4	12
300	15.2	16.2
400	18	19
Fe-3 wt% Cr		
100	4.95	5
300	16	17
400	27.8	30.5

$\langle 001 \rangle_{Fe}$ zone-axis. On this azimuth, the revealed CrN atomic planes are those of chromium which are 0.207 nm apart.

3. Local thickness of each analyzed area is estimated by exploiting Low-Loss (plasmons) EELS spectra using the relation:

$$t = \lambda \ln(I_{tot}/I_0) \tag{5}$$

where λ is the mean inelastic free path of the incident electron going trough the specimen. For iron, λ is close to 90 nm at 200 kV accelerating voltage. This value has been determined using convergent beam electron diffraction (CBED) method.

As all these parameters determined, the precipitate number per volume unit (N) and their volume fraction (f) are calculated directly using the following relations:

$$N = n/V \tag{6}$$

with $V = S \cdot T$ is the volume of the analyzed area of surface S and thickness T,

$$f = nV_p/V \tag{7}$$

with V_p the mean precipitates volume:

$$V_p = D^2 \pi t_p/4 \tag{8}$$

3. Results and discussion

3.1. Estimation of the micro-yield stress (MYS)

Fig. 4a and b show the $dr = f(F_{max})$ response of successive indentations performed at different depths on cross sections of Fe-1 wt% Cr and Fe-3 wt% Cr specimens, respectively. For the low chromium-containing alloy, one can note that the residual displacement increases continuously as a function of the maximal load as well as of depth which is compatible with the progressive diminution of the nitrogen concentration (Fig. 1).

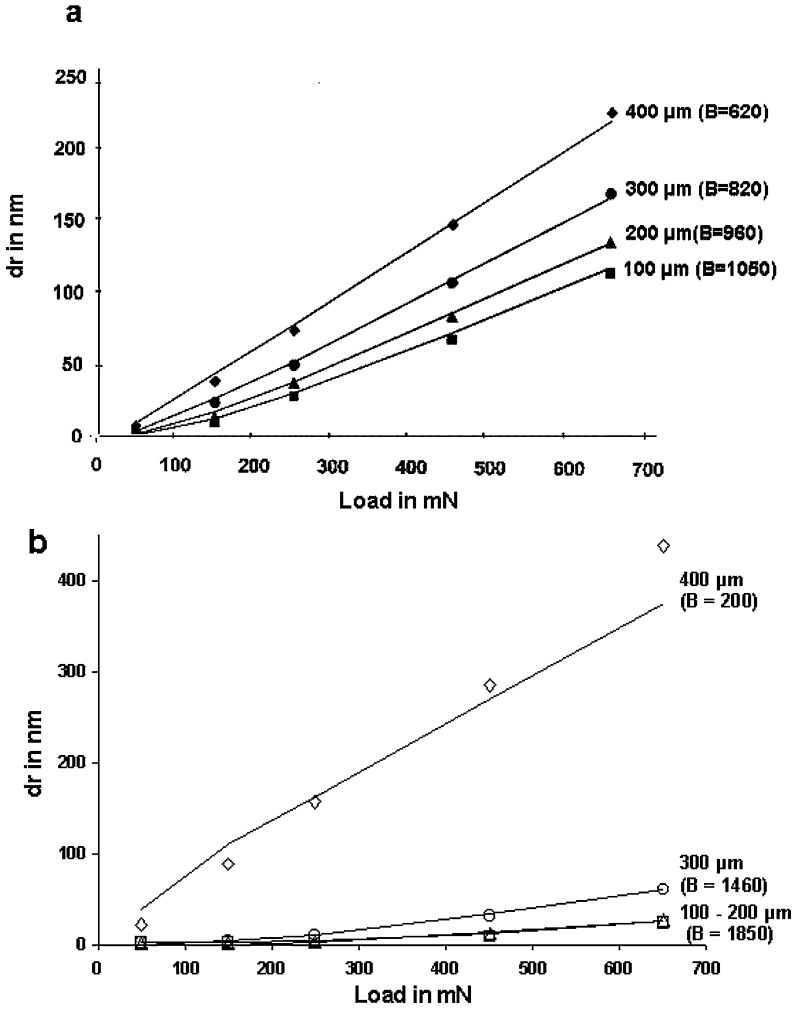

Figure 4 Indenter residual displacement (dr) as a function of maximum load F_{max}. (a) Fe-1 wt% alloy and (b) Fe-3 wt% alloy. Individual marks are experimental data; continuous lines corresponds to power law fit $dr = \alpha[2\tau_0 - B\,(C+20)^n]^\beta$ with C = 16 and n = 0.067.

TABLE III Parameters of Equation 3 where *dr* is expressed in nm, for different maximum applied loads

Maximum applied load (mN)	τ_0 (MPa)	α	β
650	2320	1.39×10^{-12}	4.02
450	2060	3.57×10^{-12}	3.92
250	1960	7.06×10^{-11}	3.87
150	1430	5.48×10^{-11}	3.95
50	988	1.13×10^{-10}	3.93

However, for the high chromium-containing alloy, the *dr* evolution as a function of the maximal load reproduces the sharp case-core observed on micro-hardness profile. Indeed, it shows two different aspects depending on the depth below the surface. First, inside superficial regions (depth <300 μm), no significant increasing of *dr* with load was measured, which is expected regarding the high hardness of these regions (>800 $Hv_{0.2}$). On the other hand, inside internal regions (depth >300 μm) where the hardness is much lower than at the surface, *dr* increases rapidly and exhibits a quasi-linear evolution as a function of the maximal load.

For both alloys, all experimental results were well fitted by the power law $dr = \alpha[2\tau_0 - B(C + 20)^n]^\beta$ with a single value for the exponent $n = 0.067$ and the parameter $C = 16$. Values of B and (τ_0, α, β) parameters depending on depth and maximum applied load, respectively, are indicated on Table III.

The misfit between experiment and simulation observed in core regions (400 μm), especially in the case of the Fe-3 wt% Cr alloy, is principally due to the fact that in these low-hardened regions, n and C terms values are no entirely valid. Indeed, both values derived from calculations performed rather for description of the hardened zone behavior.

Fig. 5a and b shows the MYS profiles of both studied alloys. It can be seen that the MYS varies practically as the micro-hardness and the nitrogen concentration although the MYS slightly decreases more rapidly than micro-hardness in the case of the 1%wt Cr alloy.

The nano-indentation tests performed in this work are concerned only with small plastic strains whose maximum value increases with an increasing applied load, reaching about 1.5% for the highest one.

Thus, the plastic strain range involved in these nano-indentation tests is at least one order of magnitude below those involved in classical hardness tests for which plastic strains usually reach 10–50% [10].

This explains why the proposed method is a good way to determine the yield stress for very small proof strains.

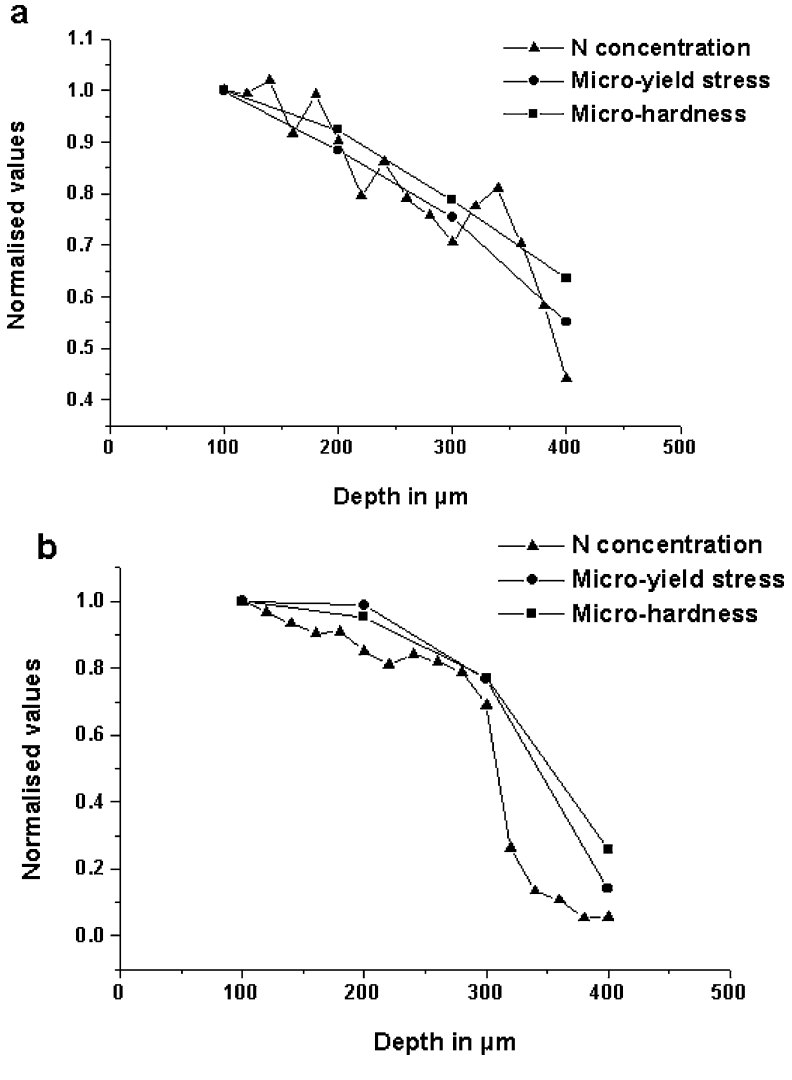

Figure 5 Comparison between micro-yield stress, micro-hardness and nitrogen concentration profiles: (a) Fe-1 wt% Cr alloy and (b) Fe-3 wt% Cr alloy.

TABLE IV Results of statistical analysis of fine CrN precipitates

	Fe-1 wt% Cr alloy			Fe-3 wt% Cr alloy		
Depth (μm)	100	300	400	100	300	400
D (nm)	12	16.2	19	5	17	30.5
t_p (nm)	0.6	0.6	0.8	0.2	1	0.5
N (10^5 pp/μm^3)	1.8	1.1	0.34	18	1.6	0.25
f (%)	1.22	0.91	0.77	0.7	3.6	0.9
f' (%)			1.64			4.9

3.2. Quantitative analysis of the CrN precipitation

All quantification results are kept on table 4 where f' represents the theoretical volume fraction of CrN precipitates corresponding to the complete precipitation of chromium from solid solution. One can note that for both alloys, an increasing of the precipitate mean diameter with depth accompanied with the decreasing of densities of precipitates per volume unit. However, it is interesting to note the particular case concerning the superficial zone in the Fe-3 wt% alloy where discontinuous precipitation is predominant. In these regions, even if the total fraction of CrN precipitates (discontinuous and continuous precipitates) is more important than in internal regions, the continuous precipitation constitutes only a very small fraction which is about 0.7% but involves a very high density of very fine ($\sim$5 nm) CrN precipitates.

3.3. Correlation with mechanical properties

Fig. 6a and b show a comparison between the evolution of the MYS and microstructural parameters through the nitrided layers for both Fe-Cr alloys. Thus, concerning Fe-1 wt% Cr alloy, the MYS varies practically like the volume fraction and inversely to the mean precipitates diameter. However, in the case of Fe-3 wt% Cr alloy, such behavior was observed only in untransformed zones ($\geq$200 μm). Indeed, inside discontinuous precipitation zone, despite the low fraction of continuous

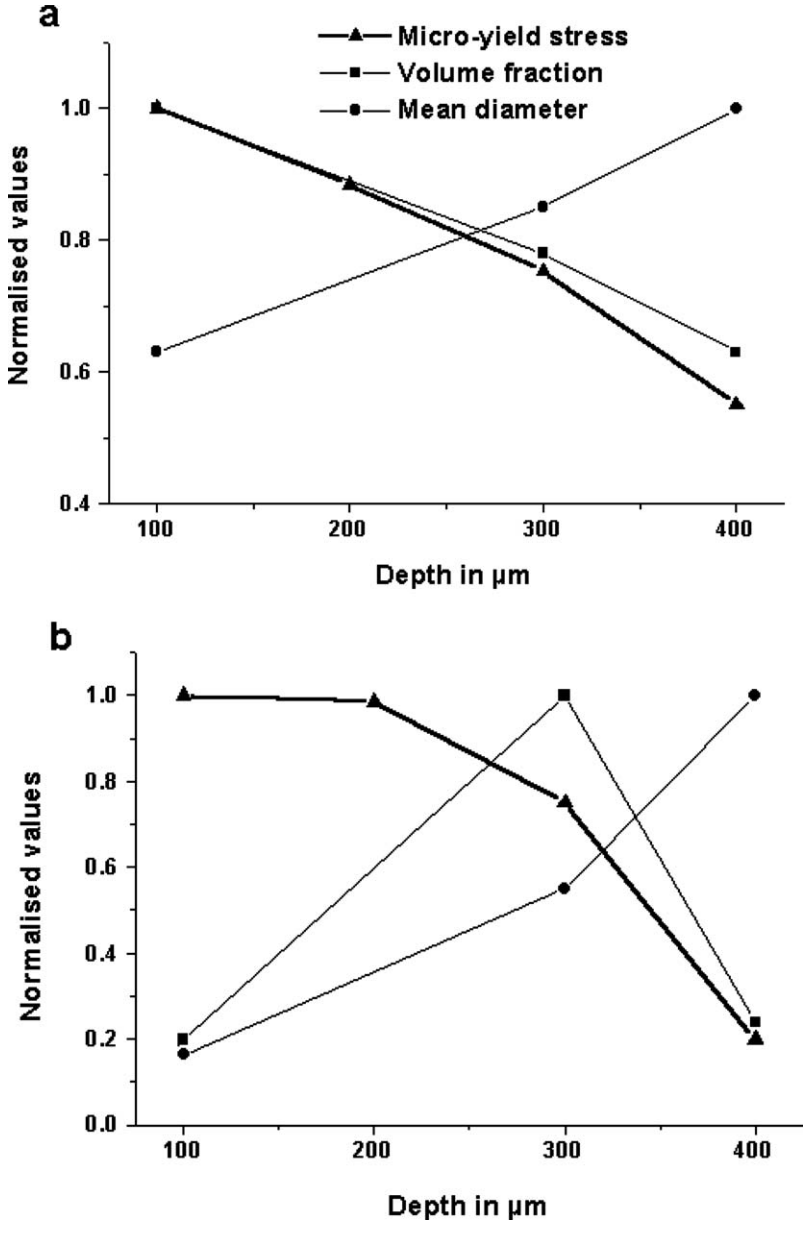

Figure 6 Comparison between micro-yield stress and microstructural parameters profiles: (a) Fe-1 wt% Cr alloy and (b) Fe-3 wt% Cr alloy.

CrN precipitates, they produce a significant strengthening which is due to their high density per volume unit which means a high number of pining points for moving dislocations.

The relation between the MYS and microstructural parameters can provide interesting information about the operating mechanism. Indeed, depending on the mechanism of the precipitates—dislocations interaction, the yield stress may be expressed as a function of the microstructural parameters into two ways [11]:

(i) *Orowan mechanism* (*skirting mechanism*)

$$\sigma_{\mathrm{Or}} \infty \frac{\Gamma f^{1/2}}{b R_{\mathrm{p}}(\pi^{1/2} - 2f^{1/2})} \cong \frac{\Gamma f^{1/2}}{b R_{\mathrm{p}} \pi^{1/2}} \qquad (9)$$

with f is the volume fraction of precipitates, Γ the line tension of dislocation, R_{p} the precipitate radius and b is the Burgers vector of mobile dislocation.

(ii) *Shearing mechanism*

$$\sigma_{\mathrm{Sh}} \infty \frac{\gamma^{3/2} R_{\mathrm{p}}^{1/2} f^{1/2}}{b \Gamma^{1/2}} \qquad (10)$$

where γ is the supplementary interfacial energy between the matrix and the precipitate, created after crossing precipitate by the moving dislocation.

Hence, in order to determine the operating mechanism in the case of both studied alloys, we have only to draw on logarithmic scales the variation of σ as a function of $(f^{1/2} * R_{\mathrm{p}}^{1/2})$ and $(f^{1/2}/R_{\mathrm{p}})$, and to see in what case the slope is close to 1.

From curves of Fig. 7a and b, it is clear that experimental results are rather in best accord with the Orowan mechanism. This is an expected result since the precipitates thickness and the strong Cr-N chemical bonding make very difficult the shearing of precipitates by the moving dislocations.

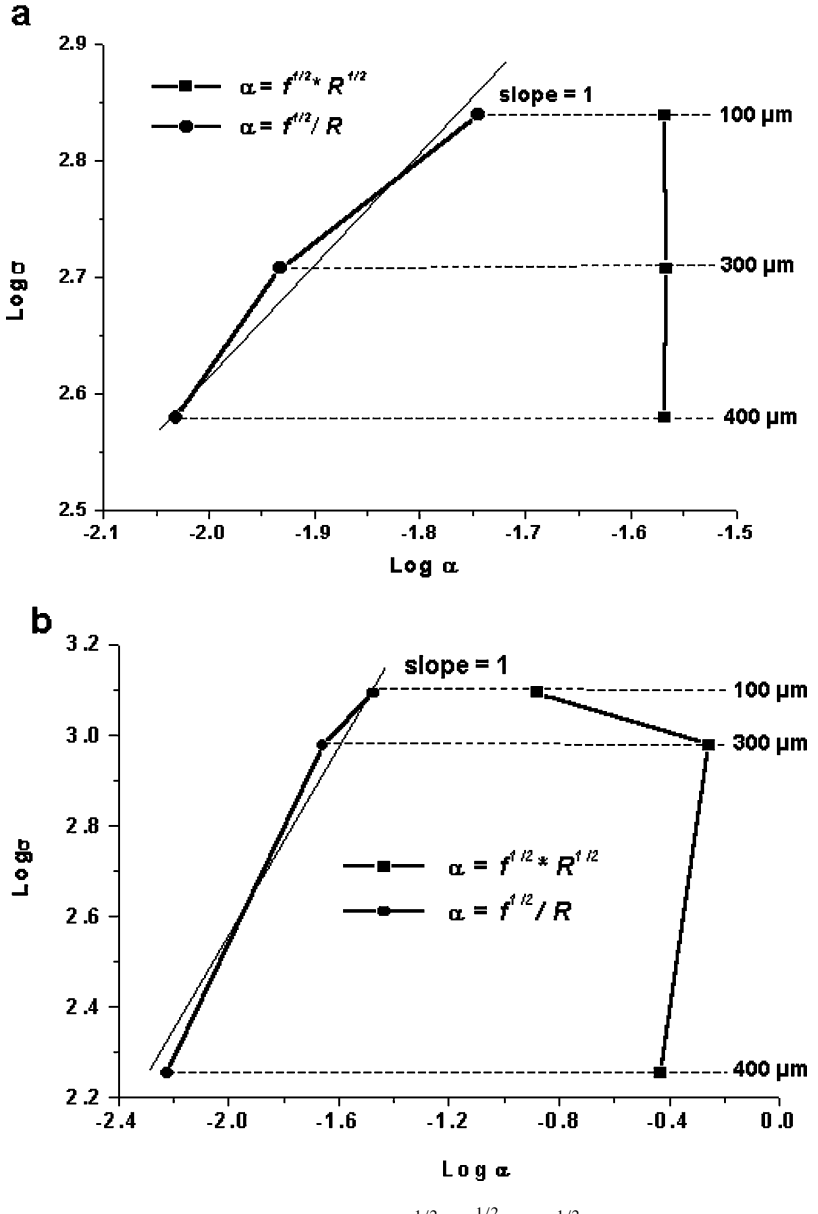

Figure 7 Micro-yield stress profiles in logarithmic scale as a function of $f^{1/2} * R_{\mathrm{p}}^{1/2}$ and $f^{1/2}/R_{\mathrm{p}}$ (a) Fe-1 wt% alloy and (b) Fe-3 wt% alloy.

4. Conclusion

Mechanical and microstructural properties of nitrided Fe-Cr layers have been investigated. The micro-yield stress (MYS) was estimated at different depths from the nitrided surface using nano-indentation test. Computational models developed in order to derive mechanical properties of 32CrMoV13 from nano-indentation tests, have been successfully applied to Fe-Cr alloys. The obtained results confirmed the decrease of the MYS with depth, in coherence with the decreasing of the nitrogen concentration.

Furthermore, a statistical analysis of the CrN precipitation has been carried out in order to interpret the profile of mechanical properties. Mean diameter, volume fraction and density per volume unit of submicroscopic nitrides were mesured at different depth in the nitrided layer from TEM observations.

The correlation between the evolution of the MYS and these microstructural parameters showed that the MYS is related to volume fraction and mean diameter of precipitates by the following relationship: MSY = Cte $(f^{1/2}/R_{\mathrm{p}})$. This behavior is rather compatible with the Orowan mechanism of precipitates hardening.

Acknowledgements

The authors would like to thank Ecole des Mines de Saint-Etienne for supplying the Fe-Cr alloys and SNR society (Annecy) for supplying the 32CrMoV13 steel and for the access to the BMI Furnace. Thanks are due to M. Pelloux for performing the nitriding treatments. We thank the Consortium Lyonnais de Microscopie Electronique (CLYME) for the access to the Jeol 2010F and Jeol 200CX microscopes.

References

1. J. GROSCH and J. MORRAL, in Proceedings of 2nd International Conference on Carburizing and Nitriding with Atmospheres, Cleveland, December 6–8, edited by M. Schneider (ASM International, 1995).
2. J. A. KNAPP, D. M. FOLLSTAEDT, F. VERGNE and A. VINCENT, *Mater. Sci. Eng.* A **215** (1996) 1460.
3. H. ELGHAZAL, G. LORMAND, A. HAMEL, D. GIRODIN and A. VINCENT, *ibid.* **303** (2001) 110.
4. C. JACQ, G. LORMAND, D. NÉLIAS, D. GIRODIN and A. VINCENT, *ibid.* **342** (2003) 311.
5. P. LAMAGNÈRE, R. FOUGÈRES, A. VINCENT, G. LORMAND, D. GIRODIN, G. DUDRAGNE and F. VERGNE, *J. Tribol.* **120** (1998) 421.
6. M. A. J. SOMERS, R. M. LANKREIJER and E. J. MITTEMEIJER, *Phil. Mag. A.* **59** (1989) 353.
7. M. SENNOUR, P. H. JOUNEAU and C. ESNOUF, submitted for publication in *J. of Materials.*
8. J. N. LOCQUET, R. L. SOTO, L. BARRALIER and A. CHARAI, *Microsc. Microanal. Microstruct.* **8** (1997) 335.
9. M. SENNOUR, PhD thesis, Lyon INSA, 2002.
10. V. YU, B. A. MILMAN, S. I. GALANOV and CHUGUNOVA, *Acta. Metall. Mater.* **41** (1993) 2523.
11. P. GUYOT, *Phil. Mag.* **24** (1971) 989.

Received 10 July 2003
and accepted 5 March 2004